Materials Today Chemistry 28 (2023) 101379

Contents lists available at ScienceDirect

Materials Today Chemistry

journal homepage: www.journals.elsevier.com/materials-today-chemistry/

Validating the reversible redox of alkali-ion disulfonyl-methanide as organic positive electrode materials

Y. Zhang [a, b], P. Apostol [b], X. Guo [b], X. Liu [b], D. Rambabu [b], J. Wang [b, ***], X. Chen [a, **], A. Vlad [b, *]

[a] College of Materials Science and Engineering, Hunan Province Key Laboratory for Advanced Carbon Materials and Applied Technology, Hunan University, Changsha, 410082, Hunan, PR China
[b] Institute of Condensed Matter and Nanosciences, Université Catholique de Louvain, Louvain-la-Neuve, Belgium

ARTICLE INFO

Article history:
Received 20 May 2022
Received in revised form
4 December 2022
Accepted 4 January 2023
Available online xxx

Keywords:
Organic battery
Aromatic disulfonyl-methanide
Alkali-ion storage
Cathode

ABSTRACT

Alkali-ion reservoir organic positive electrode materials with high redox potential emerge as promising candidates for rocking-chair batteries. Despite recent major advances on coordinated Li-enolates and conjugated Li-sulfonamides, alike chemistries remain rare with clearly enormous room to explore and investigate. Herein, we report a new high-voltage redox functionality for alkali-ion storage based on aromatic di-sulfonyl methanide. The versatile paradigm chemistry of di-alkali *p*-phenylene-bis-diethylsulfonyl methanide (denoted as A_2-*p*-$TESO_2$, where A = Li^+, Na^+, K^+) displays high voltage (3.13 vs Li^+/Li), a two-electron reversible redox in both liquid phase and solid phase electrochemistry. A_2-*p*-$TESO_2$ also shows great stability under ambient air conditions in their alkali-ion reservoir states. This work not only suggests a new charge storage mechanism for organic batteries but also highlights the versatility of organic chemistry in designing new redox functionalities for next-generation organic rechargeable batteries.

1. Introduction

Organic electrode materials (OEMs) are becoming indispensable candidates for electrochemical energy storage [1–5]. Sustainability, natural abundance, and steadily improved electrochemical performance of a variety of OEMs have generated tremendous interest on their utilization as positive electrode materials for future battery systems (redox flow cells and conventional solid cells, etc.) [6–11]. More importantly, they are not only emerging as mere alternatives to the traditional transition metal oxide cathodes in conventional rechargeable batteries, rather, have the potential to complement and lead to disruptive technologies [12–14]. Despite these excitements, however, OEMs chemistries are still in early stages of development as compared to their inorganic counterparts (e.g., $LiFePO_4$ and $Li[Ni,Co,Mn]O_2$), and the lack of suitable positive electrode materials considerably restricts their applications [15–19].

Over decades, continued exploration of organic molecules has provided bountiful possibilities for investigating their energy storage mechanism [20–23]. The broad class of OEMs can be classified into two main categories, *n*-type and *p*-type system, according to whether cations or anions are used for charge compensation upon redox [24]. The *p*-type electrode materials are usually prepared and handled in their reduced state, undergoing oxidation at the first cycle utilization, requiring thus anions for charge compensation. Consequently, such chemistries are primarily compatible with dual-ion or anionic batteries [25,26]. Given this charge storage mechanism, the *p*-type electrode materials are plagued by limited specific capacity given their high molecular weight but in particular, due to the additional large molecular weight of compensating anions (e.g., $TFSI^-$, PF_6^-) that need to be considered for capacity and energy metric calculations.

Conversely, a large part of the *n*-type electrode materials library are prepared and handled in their oxidized cation-free containing state and require initial reduction with alkali cations uptake (e.g., upon first cycle cell discharge) [1]. For a full cell assembly, this configuration inevitably requires an alkali-cation containing anode

* Corresponding author.
** Corresponding author.
*** Corresponding author.
E-mailaddresses: jiande.wang@uclouvain.be (J. Wang), xiaohuachen@hnu.edu.cn (X. Chen), alexandru.vlad@uclouvain.be (A. Vlad).

https://doi.org/10.1016/j.mtchem.2023.101379

that remains sophisticated to prepare, needs to be handled exclusively under an inert atmosphere, resulting thus in extra production costs as well as safety issues. Therefore, the optimal organic positive electrode material should be in the reduced alkali-ion containing state, namely organic alkali-ion cathodes (OAICs), alike the commercial Li-ion battery cathodes (e.g., $LiFePO_4$).

However, despite the undeniable need of OAICs chemistries, the current state-of-the-art OAICs, unlike the large diversity of inorganic ones, resume to a handful of chemistries all developed over the past 4 years. Exhilaratingly, based on decades of studying and developments, only recent advances in molecular engineering succeeded in addressing the issue of the considerably increasing the redox potential of *n*-type organic redox materials. The sulfonated analog of dilithium (2,5-dilithium-oxy)-terephthalate (denoted Li_4-*p*-DHT) [27], namely tetralithium 2,5-dihydroxy-1,4-benzenedisulfonate (Li_4-*p*-DHBDS) [28], developed by Lakraychi et *al*. provided a discharge potential as high as ~3.25 V (vs. Li^+/Li), making it the first organic and lithiated positive electrode material processable under dried air. Shortly after, Poizot et al. demonstrated that substituting two Li^+ by Mg^{2+} in parent Li_4-*p*-DHT, resulting in $Li_2(Mg)$-*p*-DHT, enabled a net voltage gain of nearly +800 mV, providing a battery material operating at 3.35 V (vs. Li^+/Li) [29]. Afterward, the exotic chemistry of tetralithium 2,5-dihydroxy-1,4-benzenediacetate (Li_4-*p*-DOBDA) was disclosed with remarkable air stability and high redox potential, arising from a peculiar molecular arrangement and reactivity in the solid phase [30] (Scheme 1, top panel). However, the structural and compositional expandable space for OAICs remains limited due to extensive reliance on enolate-carbonyl electrochemistry that intrinsically operates at relatively lower redox potential.

The limitations of the carbonyl-based redox chemistries have been thus the motivation for designing new organic redox active materials with *n*-type characteristics. Wang et al. recently reported the conjugated sulfonamide chemistry, disclosing as many as eight derivate chemistries with Li-reservoir with excellent moisture and oxygen resistance, as well as versatility for different alkali cation storage (Scheme 1, middle panel) [31,32]. The existing research achievements remain however minimal as compared to the broad and diverse library of inorganic materials so that the bottlenecks at hand prompted us to explore, investigate, and analyze further new OAIC chemistries.

In this work, we report a new OAICs redox center based on conjugated alkali-ion disulfonyl-methanide (Scheme 1, **bottom panel**). The disclosed *p*-phenylene-bis-(diethylsulfonyl methide) with various alkali-ions (A_2-*p*-$TESO_2$, A = Li^+, Na^+, K^+) display a two-electron reversible redox in both liquid and solid state electrochemical systems, switching between the reduced methanide and oxidized methide forms. As a universal positive electrode material, their alkali-reservoir feature, high redox potential, and remarkable air stability make this new redox chemistry interesting and promising for alkali-ion storage in conventional alkali-ion cells. The high solubility of both oxidized and reduced phase may make this new chemistry particularly interesting as catholyte for alkali-ion supercapacitor as well as redox flow systems. With this finding, we enrich the organic alkali-ion-containing electron storage mechanism and further offer new directions and principles for developing and improving organic materials for energy storage applications.

2. Results and discussions

The synthesis of α, α, α′, α′-tetrakis-(ethylsulfonyl)-*p*-xylene (H_2-*p*-$TESO_2$) was adapted from a previously publication [33] and details are provided in Scheme 2. The deprotonation (e.g. lithiation, sodiation, and potassiation) was carried out by reacting H_2-*p*-$TESO_2$ with stoichiometric amounts of respective alkali-ion tert-butoxide in anhydrous tert-butyl alcohol under an inert atmosphere (refer to SI for detailed synthesis process). The successful deprotonation was confirmed by the disappearance of the −CH characteristic peaks of ^1H NMR in A_2-*p*-$TESO_2$ (A = Li^+, Na^+, K^+) compared to H_2-*p*-$TESO_2$, as well as the shielding effect on all protons attributed to the increased electron density upon the formation of the di-anionic specie (Fig. 1a and Fig. S1-S3). Red shift of $\nu_{sym}(SO_2)$ and $\nu_{asym}(SO_2)$ bands is also observed in Fourier-transform infrared

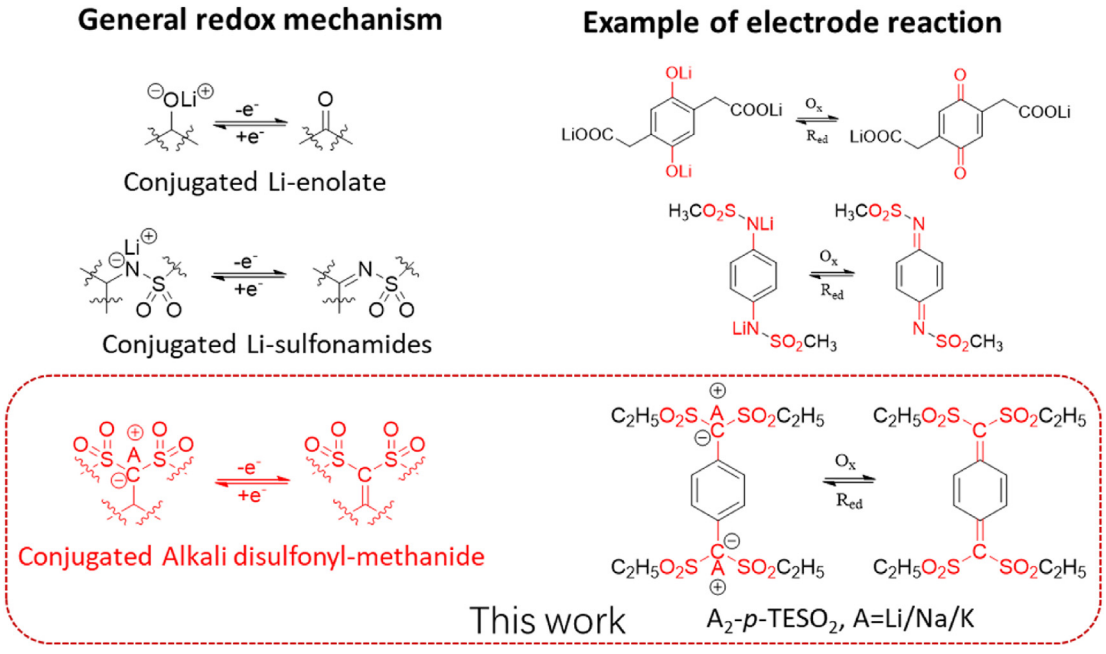

Scheme 1. Reaction mechanisms of reported Li-containing organic positive electrode chemistries and their paradigms. Top panel: conjugated Li-enolate; middle panel: conjugated Li-sulfonamide; bottom panel: conjugated alkali-ion disulfonyl-methanide in this work.

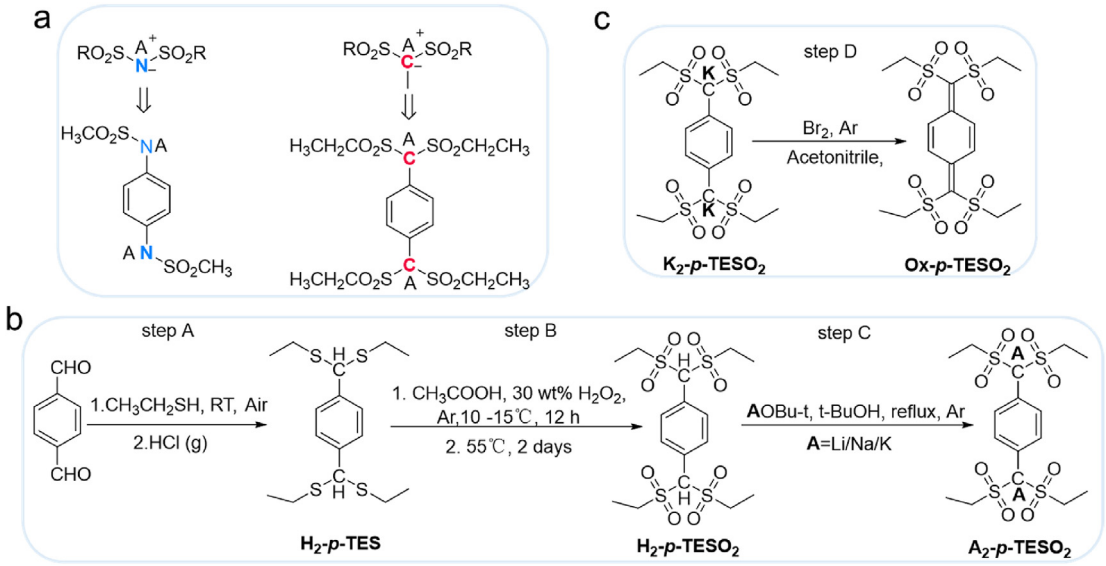

Scheme 2. The design rational and synthesis pathways for A_2-*p*-$TESO_2$ and Ox-*p*-$TESO_2$, A = Li, Na, K. (a) the design of A_2-*p*-$TESO_2$ based on similar rational of Li_2-*p*-PDSA; (b) Synthesis procedure of A_2-*p*-$TESO_2$. (c) The oxidation of K_2-*p*-$TESO_2$ to Ox-*p*-$TESO_2$.

spectroscopy (FTIR) of due to the corresponding electronic effect upon deprotonation (Fig. 1b).

Generally, the ternary $(R)_3$-CH protons show a low ^{1}H NMR chemical shift of around 2–5 ppm, indicating strong difficulty to deprotonate. In the case of H_2-*p*-$TESO_2$, the strong electron withdrawing effect of the sulfonyl groups induces high electronic delocalization, altering the proton chemical shift deshielding to 6.70 ppm (Fig. S2). This is an indication of increased acidity of the −CH, leading to the deprotonation (e.g. lithiation, sodiation, and potassiation) being possible via acid−base reaction.

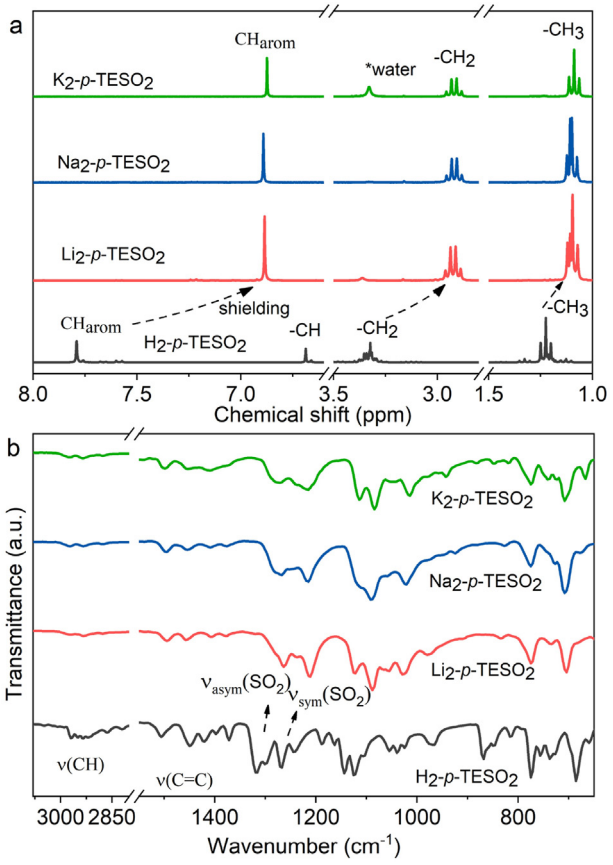

Fig. 1. Deprotonation process of H_2-*p*-$TESO_2$: (a) ^{1}H NMR spectra before and after deprotonation, (b) FTIR survey data of A_2-*p*-$TESO_2$ (A = Li, Na, K) materials as compared to parent H_2-*p*-$TESO_2$.

The prepared A_2-*p*-$TESO_2$ (A = Li, Na, K) compounds were further characterized by powder X-ray diffraction (PXRD), displaying higher crystallinity for the potassium analog and more disordered for lithium and sodium versions (Fig. S5). Similar trends were already noted in other chemistries including both organic (Li_4/Na_4/K_4-PTtSA) [32] and inorganic (Li_2/Na_2/K_2MoS_4) [34] materials, whereas the bonding strength and cations radius are plausible explanations of such correlation, however requiring further investigation for clearly understanding the effects. Air stability is a parameter that not only indicates the potentially practical application of an electrode material by reducing the cost of processing but also implies a high redox potential given the O_2 oxidation potential of ~2.91 V vs. Li^+/Li. Motivated by this, the air stability of A_2-*p*-$TESO_2$ materials was evaluated by comparing the FTIR of the pristine sample and the sample exposed to ambient atmosphere. All A_2-*p*-$TESO_2$ compounds displayed excellent tolerance to molecular oxygen and moisture, with negligible changes in FTIR spectra (Fig. S6). This is not only a practical feature for handling and processing the electrode materials but also indirectly suggesting a high oxidation potential (>2.91 V vs. Li^+/Li) of these materials.

With the structural and composition features of these materials identified, we next studied the electrochemistry and charge storage performances. The electrochemical reversibility and determination of the redox potential were first characterized by cyclic voltammetry in dissolved form (Fig. 2). When compared to its closest sulfonamide analog (the dilithium 1,4-phenylenebis((methyl sulfonyl)amide) Li_2-*p*-PDSA) with a similar two-electron reversible redox (through *p*-sulfonamide/quinoneimine couple), the Li_2-*p*-$TESO_2$ displays an increase in redox potential by as much as 300 mV (Fig. 2a, b). This can be explained by the presence of four electron-withdrawing sulfonyl groups (−SO_2−) bonded to the tetravalent carbon compared to only two sulfonyl groups in Li_2-*p*-PDSA, leading to enhanced electronic delocalization by mesomeric effect (-M), stabilizing the dianion, and thus resulting in a higher redox

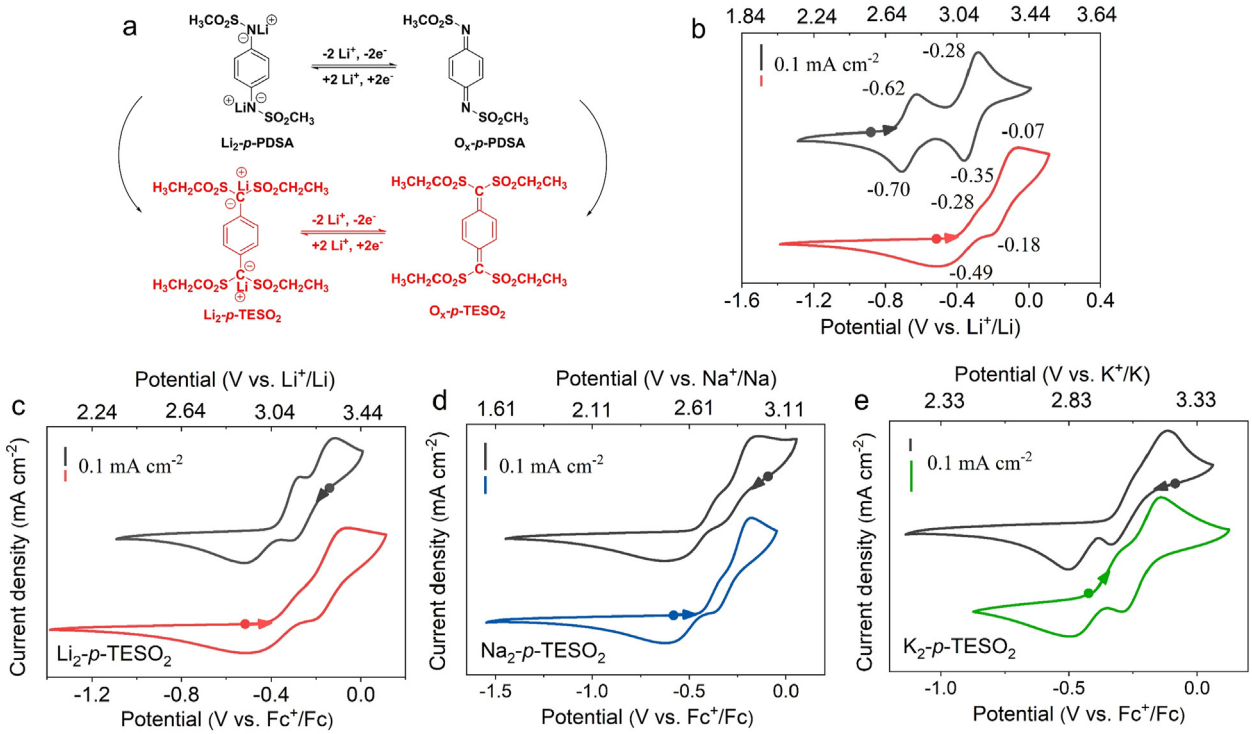

Fig. 2. Comparative illustration of (a) redox mechanism and (b) liquid cyclic voltammetry (CV) between Li_2-*p*-PDSA (black curve) and Li_2-*p*-$TESO_2$ (red curve). The Li_2-*p*-PDSA data are reproduced from Ref. [31]. CV scans of (c) Li_2-*p*-$TESO_2$, (d) Na_2-*p*-$TESO_2$, and (e) K_2-*p*-$TESO_2$; along with the CV data of Ox-*p*-$TESO_2$ for each system (black lines). Measurement conditions are 5 mM of active material dissolved in electrolyte made of 0.1 M of carrier ATFSI salt (A = Li^+, Na^+, K^+) in N,N-dimethylformamide (DMF) solvent. Data acquired at a scan rate of 100 mV s^{-1}, on a platinum working electrode. The electrode potential was measured vs. a silver reference electrode, calibrated with an Fc^+/Fc internal standard.

potential. This is indeed a significant phenomenon, showing that with electronic effect of different substituents, redox potential of organic electrode molecules can be further increased.

To further elucidate and corroborate the redox mechanism of the A_2-*p*-$TESO_2$ series, the oxidized form (noted as Ox-*p*-$TESO_2$) was chemically synthesized and isolated as a pure and stable phase (refer to Figs. S4, S5, S7 for details) [33]. As shown in Fig. 2c, both Li_2-*p*-$TESO_2$ and Ox-*p*-$TESO_2$ display distinct reversible molecular electrochemistry with two pairs of overlapping redox peaks, indicative of a sequential two-electron redox behavior of these

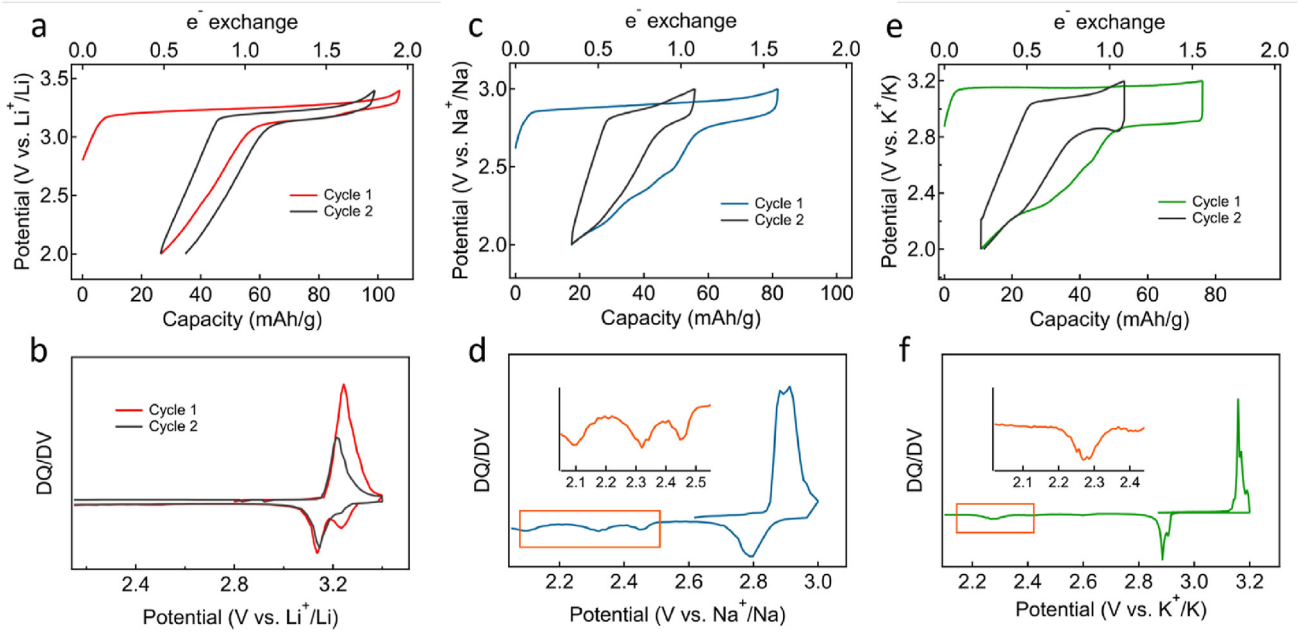

Fig. 3. The electrochemistry of A_2-*p*-$TESO_2$ in solid cells. Potential vs. capacity galvanostatic curves acquired at a rate of 0.1C for (a) Li_2-*p*-$TESO_2$, (c) Na_2-*p*-$TESO_2$, and (e) K_2-*p*-$TESO_2$ electrode materials. The differential capacity function of potential plots (dQ/dV vs. V) for the respective cells: (b) Li_2-*p*-$TESO_2$, (d) Na_2-*p*-$TESO_2$, and (f) K_2-*p*-$TESO_2$.

redox centers. The anodic process is assigned to the electrochemical formation of the radical anion form at 3.15 V (vs. Li^+/Li) followed by the formation of the neutral oxidized state at 3.30 V (vs. Li^+/Li). The two processes are reversible, with the cathodic peaks located at 3.20 V and 3.00 V (vs. Li^+/Li), respectively. The sodium and potassium salts also show similar two-electron reversible cyclic voltammetry responses. The high redox potential of A_2-*p*-$TESO_2$ corroborates the observed excellent stability toward oxygen. The high reversibility of A_2-*p*-$TESO_2$ directly confirms that the conjugated disulfonyl-methanide as a universal organic positive electrode material can support two-electron redox for alkali-cation storage (Fig. 2d and e), where the redox pathway is between the reduced disulfonyl-methanide and oxidized *p*-quinomethane forms (Fig. 2a).

The solid phase electrochemical behavior of A_2-*p*-$TESO_2$ materials was characterized next in half cell configuration, with the respective alkali-metal (Li, Na, or K) as counter and pseudo-reference electrodes, and the results are resumed in Fig. 3. The potential capacity plots for Li_2-*p*-$TESO_2$/Li cell cycled at a rate of one lithium-ion in 5 h (equivalent of 0.1C rate), with a cutoff potential between 2.0 and 3.4 V vs. Li^+/Li are shown in Fig. 3a. At the first charge step, the potential initially rises sharply to reach a plateau located at 3.26 V (vs. Li^+/Li) corresponding to an overall extraction of nearly two electrons/Li^+ per formula unit. Upon discharge, the electrode potential traces back the charge profile with a small polarization of ~100 mV, remaining 75% reversible capacity (Fig. 3a and b). In addition, the Li_2-*p*-$TESO_2$/Li cell was characterized with larger potential window of 2.0–3.7 V. Upon charging, a second small charge plateau appears at high potential of 3.5 V; however, during the following discharge, the plateau around 3.10 V disappears and a new one appears at a lower value of 2.50 V vs. Li^+/Li (Fig. S8a). This phenomenon is probably due to the decomposition of the electrode material at high operation voltage.

For the sodium and potassium analogs, both display similar two-electron first charging process with flat charge plateaus at 2.98 V vs. Na^+/Na and 3.10 V vs. K^+/K, respectively (Fig. 3c–f). The discharge process is also characterized by a lower capacity supplied at high potential (less than one electron exchange) for both Na_2-*p*-$TESO_2$/Na and K_2-*p*-$TESO_2$/K cells, accompanied by a second plateaus at lower potentials. More discussion and explanation will be given for the origins of this partial reversibility and redox potential change. At this stage, we believe this is attributed to partial molecular decomposition during charge process. This is further indirectly corroborated by increasing the charge potential to higher

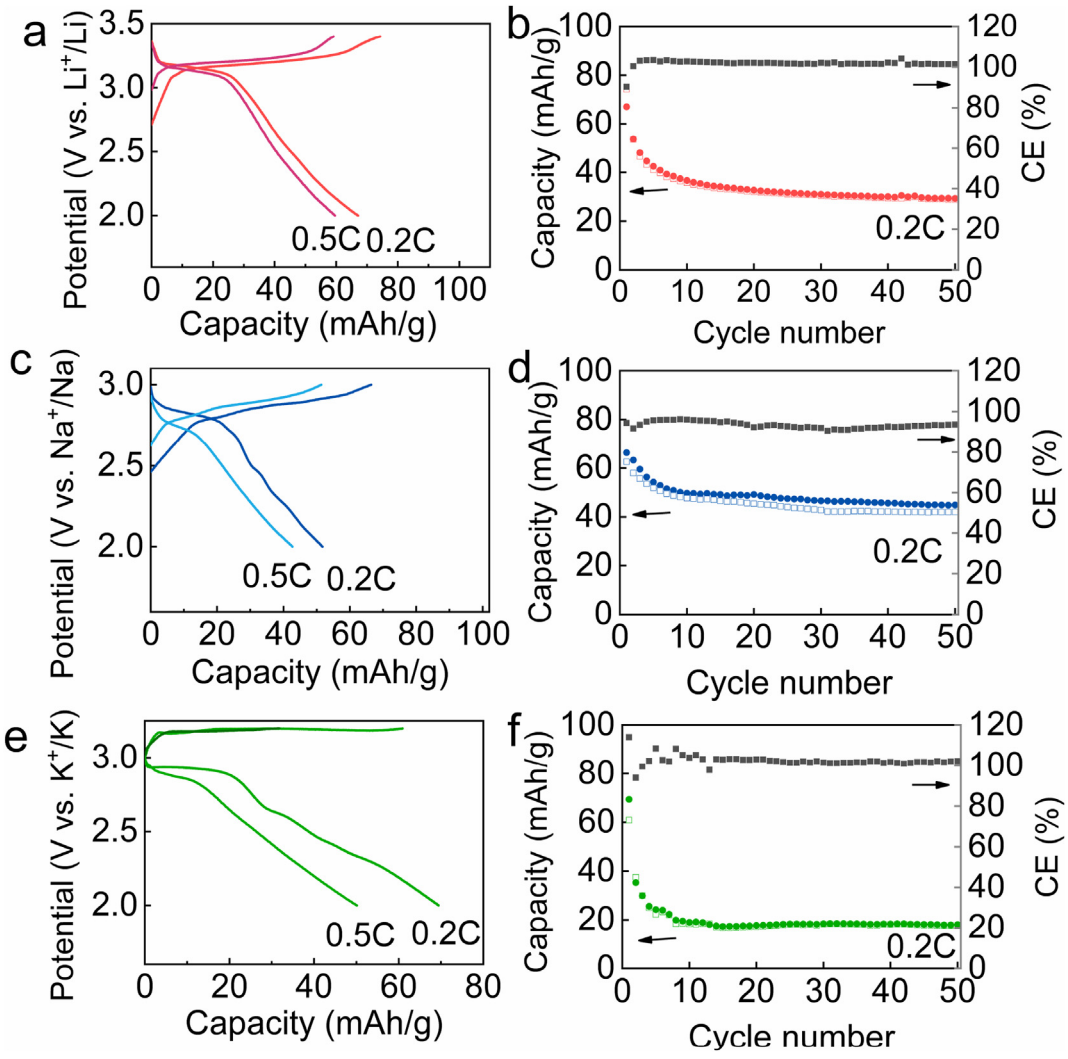

Fig. 4. Rate and cycling performance of A_2-*p*-$TESO_2$ in solid cells. (a, b) Li_2-*p*-$TESO_2$, (c, d) Na_2-*p*-$TESO_2$, and (e, f) K_2-*p*-$TESO_2$ electrode.

Table 1
Comparison of average discharge and charge voltage of A_2-p-$TESO_2$ materials as measured in solid (s, based on data from Fig. 3) and liquid states (l, based on data from Fig. 2).

	Redox potential (Solid, V vs. A^+/A)	Redox potential (Liquid, V vs. Fc^+/Fc)
Li_2-*p*-$TESO_2$	3.13	−0.28
Na_2-*p*-$TESO_2$	2.81	−0.40
K_2-*p*-$TESO_2$	2.98	−0.31

values (>3.0 V vs. Na^+/Na and >3.2 V vs. K^+/K), where only the low potential discharge profile was retained, indicating the complete decomposition of the materials (Figs. S8b and S8c). Meanwhile, an interesting voltage hysteresis phenomenon was observed in A_2-*p*-$TESO_2$ materials during charge−discharge process in solid-state. In our previous work of Li_2-*p*-PDSA, Li_2-*p*-PDSA also showed similar first cycle hysteresis [31]. According to our investigation, the hysteresis is due to the nucleophilic attack to the free aromatic positions in the fully oxidized state. Once the 2, 5 aromatic positions were protected, hysteresis phenomenon disappears. In this work, since A_2-*p*-$TESO_2$ share similar molecular structure as well as electrochemical redox mechanism, we believe it is highly possible that similar electrochemically induced Michael-type addition also happens in the oxidized state of A_2-*p*-$TESO_2$. Indeed, similar behavior is known from flow battery research on quinone derivatives, many of these shown to undergo Michael reaction in b-position when operated in aqueous media [35,36], unless this position is substituted [37]. However, it is still unknown why this phenomenon only happens in the solid state instead of liquid state in the case of A_2-*p*-$TESO_2$. Thus, more investigation is needed to understand this interesting phenomenon.

With the origins of the reversible redox reaction of A_2-*p*-$TESO_2$, we next discuss the rate and cycling performance of A_2-*p*-$TESO_2$ in solid cells. Considering the solubility issues (Fig. S10), here we select the first charge/discharge curve of different cells to evaluate the rate capability. The rate capability was investigated under different cycling rates of 0.2C and 0.5C. As shown in Fig. 4a, c and 4e, the reversible capacity is decreased with increasing the cycling rates and but the charge−discharge plateaus maintain. In addition, as shown in Fig. 4b, d and 4f, all the cells show fast capacity decay in the first 10 cycles attributed to the high dissolution of the active materials in liquid electrolyte and then stabilize over 50 cycles at 0.2C. Due to the relatively high solubility of A_2-*p*-$TESO_2$, we believe alkali-ion batteries are probably not the promising application for this material. Instead, this material shows high potential in their dissolved phases and might be interesting to be used as catholyte for either redox-flow batteries or alkali-ion supercapacitors thanks to their high redox potential.

It is worth noting that the most interesting feature of A_2-*p*-$TESO_2$ chemistry is the high redox potential attained, compared to other alkali-cation reservoir cathodes. As summarized in Table 1, we compare the average redox potentials of A_2-*p*-$TESO_2$ chemistries in solid (s) and liquid states (l). For Li_2-*p*-$TESO_2$, the average redox potential center at 3.13 V vs. Li^+/Li. These performances are comparable to the best Li-containing organic cathodes materials while relying on a new redox mechanism with potential for further improvements (Table S2) [24,27−31,38]. Furthermore, Na_2-*p*-$TESO_2$ is found to display an average redox potential around 2.81 V vs. Na^+/Na. Compared to reported Na-containing OEMs (Table S3) [32,39], the average redox potential of Na_2-*p*-$TESO_2$ is the highest attained so far (2.3 V vs. Na^+/Na for Na_4DHTPA [24], 2.5 V vs. Na^+/Na for Na_4-PTtSA) [32]. Finally, the average redox potential of K_2-*p*-$TESO_2$ is 2.98 V vs. K^+/K, higher than K_4-PTtSA (2.6 vs. K^+/K) [32], which is the first K-reservoir organic cathode (Table S4).

3. Conclusion

With this work, we disclose a new organic cathode material based on the reversible redox of conjugated disulfonyl-methanide (*p*-$TESO_2$). Relying on same organic center, Li-, Na-, and K-ion containing phases are prepared and studied in detail for the respective alkali-ion storage. All phases are found to be air-stable in the alkali cation reservoir form, an appealing feature for practical application, synthesis, and use. The *p*-$TESO_2$ center displays a reversible two-electrons redox per formula unit in dissolved state, whereas a more complex behavior is observed in solid phase, with only half the capacity being recovered at high potential, and more capacity being extracted at lower potential. Despite, the measured average discharge potentials are comparable as well as beyond the state-of-art of 3.13 V (vs. Li^+/Li), 2.81 V (vs. Na^+/Na), and 2.98 V (vs. K^+/K), for Li_2-, Na_2-, and K_2-*p*-$TESO_2$ phases, respectively. This new redox chemistry can be widely used in alkali-ion organic batteries. Due the high solubility, A_2-*p*-$TESO_2$ might not suitable for alkali-ion batteries, but more interesting as catholyte for redox-flow battery or alkali-ion supercapacitor.

Declaration of competing interest

The authors declare that they have no known competing financial interests or personal relationships that could have appeared to influence the work reported in this paper.

Data availability

Data will be made available on request.

Acknowledgments

Y.Z., X.G., X.L., and J.W. gratefully acknowledge CSC for financial support. A.V. is indebted to the European Research Council (ERC) under the European Union's Horizon 2020 research and innovation program (grant agreement no. 770870).

Appendix A. Supplementary data

Supplementary data to this article can be found online at https://doi.org/10.1016/j.mtchem.2023.101379.

References

[1] Y. Lu, J. Chen, Prospects of organic electrode materials for practical lithium batteries, Nat. Rev. Chem 4 (3) (2020) 127−142.
[2] P. Poizot, J. Gaubicher, S. Renault, L. Dubois, Y. Liang, Y. Yao, Opportunities and challenges for organic electrodes in electrochemical energy storage, Chem. Rev. 120 (14) (2020) 6490−6557.
[3] K. Qin, J. Huang, K. Holguin, C. Luo, Recent advances in developing organic electrode materials for multivalent rechargeable batteries, Energy Environ. Sci. 13 (11) (2020) 3950−3992.
[4] J. Wang, A. Vlad, Empowering magnesium, Nat. Energy 5 (12) (2020) 945−946.
[5] A.E. Lakraychi, F. Dolhem, A. Vlad, M. Becuwe, Organic negative electrode materials for metal-ion and molecular-ion batteries: progress and challenges from a molecular engineering perspective, Adv. Energy Mater. 11 (32) (2021).
[6] B. Esser, F. Dolhem, M. Becuwe, P. Poizot, A. Vlad, D. Brandell, A perspective on organic electrode materials and technologies for next generation batteries, J. Power Sources 482 (2021).
[7] B. Ernould, L. Sieuw, G. Barozzino-Consiglio, J.-F. Gohy, A. Vlad, Negative redox potential shift in fire-retardant electrolytes and consequences for high-energy hybrid batteries, ACS Appl. Energy Mater. 2 (11) (2019) 7879−7885.
[8] X. Xiong, W. Yan, Y. Zhu, L. Liu, L. Fu, Y. Chen, N. Yu, Y. Wu, B. Wang, R. Xiao, $Li_4Ti_5O_{12}$ coating on copper foil as ion redistributor layer for stable lithium metal anode, Adv. Energy Mater. 12 (13) (2022).
[9] X. Zhang, Z. Cui, A. Manthiram, Insights into the crossover effects in cells with high-nickel layered oxide cathodes and silicon/graphite composite anodes, Adv. Energy Mater. 12 (14) (2022).

[10] S. Tang, L. Li, H. Ren, Q. Lv, R. Lv, Sodium-ion electrochemical tuning of Prussian blue analog as an efficient oxygen evolution catalyst, Mater. Today Chem. 12 (2019) 71–77.
[11] Q. He, H. Wang, X. Zhao, L. Chen, Recent advances of transition metal oxalate-based micro- and nanomaterials for electrochemical energy storage: a review, Mater. Today Chem. 22 (2021).
[12] X. Judez, L. Qiao, M. Armand, H. Zhang, Energy density assessment of organic batteries, ACS Appl. Energy Mater. 2 (6) (2019) 4008–4015.
[13] Y. Liang, Y. Yao, Positioning organic electrode materials in the battery landscape, Joule 2 (9) (2018) 1690–1706.
[14] R. Rupp, A. Vlad, On the reliability of sodium metal anodes: the influence of neglected parameters, J. Electrochem. Soc. 166 (14) (2019) A3122–A3131.
[15] T.B. Schon, B.T. McAllister, P.F. Li, D.S. Seferos, The rise of organic electrode materials for energy storage, Chem. Soc. Rev. 45 (22) (2016) 6345–6404.
[16] X. Liu, J. Wang, M. Du, Q. Zhu, K. Robeyns, X. Zhang, V. Kumar, J.F. Gohy, Y. Garcia, A. Vlad, Unlocking the electrochemistry and the activation mechanism in the iron-rich $Na_{0.6}Fe_{1.2}PO_4$ phase for high-performance sodium-ion storage, Batteries & Supercaps 5 (5) (2022).
[17] Y. Zhang, Y. Yang, C. Huang, J. Wang, X. Liu, P. Apostol, A. Hu, J. Wang, X. Chen, J. Wang, Sulfur cathodes based on dual-functional GMs-MnOOH for high performance lithium sulfur batteries, Mater. Today Commun. 29 (2021).
[18] Y. Zhang, Y. Yang, C. Huang, H. Fan, D. Yuan, W.-B. Luo, A. Hu, Q. Tang, X. Chen, Understanding the effect of I/N dual-doped hard carbon for high performance K-ion storage, Electrochim. Acta 394 (2021).
[19] Y. Zhang, X. Duan, J. Wang, C. Wang, J. Wang, J. Wang, J. Wang, Natural graphene microsheets/sulfur as Li-S battery cathode towards >99% coulombic efficiency of long cycles, J. Power Sources 376 (2018) 131–137.
[20] Y. Lu, Q. Zhang, L. Li, Z. Niu, J. Chen, Design strategies toward enhancing the performance of organic electrode materials in metal-ion batteries, Chem 4 (12) (2018) 2786–2813.
[21] Y. Tian, G. Zeng, A. Rutt, T. Shi, H. Kim, J. Wang, J. Koettgen, Y. Sun, B. Ouyang, T. Chen, Z. Lun, Z. Rong, K. Persson, G. Ceder, Promises and challenges of next-generation "beyond Li-ion" batteries for electric vehicles and grid decarbonization, Chem. Rev. 121 (3) (2021) 1623–1669.
[22] H. Kim, J.E. Kwon, B. Lee, J. Hong, M. Lee, S.Y. Park, K. Kang, High energy organic cathode for sodium rechargeable batteries, Chem. Mater. 27 (21) (2015) 7258–7264.
[23] A.E. Lakraychi, S. De Kreijger, D. Gupta, B. Elias, A. Vlad, Phendione-transition-metal complexes with bipolar redox activity for lithium batteries, ChemSusChem 13 (9) (2020) 2225–2231.
[24] S. Gottis, A.L. Barres, F. Dolhem, P. Poizot, Voltage gain in lithiated enolate-based organic cathode materials by isomeric effect, ACS Appl. Mater. Interfaces 6 (14) (2014) 10870–10876.
[25] A. Jouhara, E. Quarez, F. Dolhem, M. Armand, N. Dupre, P. Poizot, Tuning the chemistry of organonitrogen compounds for promoting all-organic anionic rechargeable batteries, Angew Chem. Int. Ed. Engl. 58 (44) (2019) 15680–15684.
[26] H. Jia, T. Quan, X. Liu, L. Bai, J. Wang, F. Boujioui, R. Ye, A. Vlad, Y. Lu, J.-F. Gohy, Core-shell nanostructured organic redox polymer cathodes with superior performance, Nano Energy 64 (2019), 103949.
[27] S. Renault, S. Gottis, A.-L. Barrès, M. Courty, O. Chauvet, F. Dolhem, P. Poizot, A green Li-organic battery working as a fuel cell in case of emergency, Energy Environ. Sci. 6 (7) (2013).
[28] A.E. Lakraychi, E. Deunf, K. Fahsi, P. Jimenez, J.P. Bonnet, F. Djedaini-Pilard, M. Bécuwe, P. Poizot, F. Dolhem, An air-stable lithiated cathode material based on a 1,4-benzenedisulfonate backbone for organic Li-ion batteries, J. Mater. Chem. 6 (39) (2018) 19182–19189.
[29] A. Jouhara, N. Dupre, A.C. Gaillot, D. Guyomard, F. Dolhem, P. Poizot, Raising the redox potential in carboxyphenolate-based positive organic materials via cation substitution, Nat. Commun. 9 (1) (2018) 4401.
[30] L. Sieuw, A.E. Lakraychi, D. Rambabu, K. Robeyns, A. Jouhara, G. Borodi, C. Morari, P. Poizot, A. Vlad, Through-space charge modulation overriding substituent effect: rise of the redox potential at 3.35 V in a lithium-phenolate stereoelectronic isomer, Chem. Mater. 32 (23) (2020) 9996–10006.
[31] J. Wang, A.E. Lakraychi, X. Liu, L. Sieuw, C. Morari, P. Poizot, A. Vlad, Conjugated sulfonamides as a class of organic lithium-ion positive electrodes, Nat. Mater. 20 (5) (2021) 665–673.
[32] J. Wang, X. Liu, H. Jia, P. Apostol, X. Guo, F. Lucaccioni, X. Zhang, Q. Zhu, C. Morari, J.-F. Gohy, A. Vlad, A high-voltage organic framework for high-perfsormance Na- and K-ion batteries, ACS Energy Lett. (2022) 668–674.
[33] H. Walterr, B. Richarde, Substituted quinodimethans. IV. 7,7,8,8-Tetrakis-(ethylsulfonyl)-quinodimethan, J. Am. Chem. Soc. 84 (1962) 3474–3478.
[34] Q. Zhu, J. Wang, X. Liu, N. Ebejer, D. Rambabu, A. Vlad, Mixed anionic and cationic redox chemistry in a tetrathiomolybdate amorphous coordination framework, Angew Chem. Int. Ed. Engl. 59 (38) (2020) 16579–16586.
[35] K. Wedege, E. Drazevic, D. Konya, A. Bentien, Organic redox species in aqueous flow batteries: redox potentials, chemical stability and solubility, Sci. Rep. 6 (2016), 39101.
[36] D.P. Tabor, R. Gómez-Bombarelli, L. Tong, R.G. Gordon, M.J. Aziz, A. Aspuru-Guzik, Mapping the frontiers of quinone stability in aqueous media: implications for organic aqueous redox flow batteries, J. Mater. Chem. 7 (20) (2019) 12833–12841.
[37] L. Hoober-Burkhardt, S. Krishnamoorthy, B. Yang, A. Murali, A. Nirmalchandar, G.K.S. Prakash, S.R. Narayanan, A new michael-reaction-resistant benzoquinone for aqueous organic redox flow batteries, J. Electrochem. Soc. 164 (4) (2017) A600–A607.
[38] A.L. Barres, J. Geng, G. Bonnard, S. Renault, S. Gottis, O. Mentre, C. Frayret, F. Dolhem, P. Poizot, High-potential reversible Li deintercalation in a substituted tetrahydroxy-p-benzoquinone dilithium salt: an experimental and theoretical study, Chemistry 18 (28) (2012) 8800–8812.
[39] S. Wang, L. Wang, Z. Zhu, Z. Hu, Q. Zhao, J. Chen, All organic sodium-ion batteries with $Na_4C_8H_2O_6$, Angew. Chem. 126 (23) (2014) 6002–6006.